The effect of electrolysis conditions with different electrolyte compositions on the growth kinetics, phase-structural state, and hardness of coatings obtained by microarc oxidation (MAO) on the D16 aluminum alloy (base – aluminum, main impurity Cu) was studied.

An analysis of the results obtained showed that the choice of the type of electrolyte and the conditions for the MAO process makes it possible to vary the growth kinetics and phase-structural state of the coating on the D16 aluminum alloy within a wide range. For all types of electrolytes, with an increase in the content of KOH, Na_2SiO_3, or KOH+Na_2SiO_3, the growth rate of MAO coatings increases.

It was found that in MAO coatings obtained in an alkaline (KOH) electrolyte, a two-phase (γ–Al_2O_3 and α–Al_2O_3 phases) crystalline state is formed. An increase in the KOH concentration leads to an increase in the relative content of the α–Al_2O_3 phase (corundum). During the formation in a silicate electrolyte, the phase composition of MAO coatings with an increase in the content of liquid glass (Na_2SiO_3) changes from a mixture of the γ–Al_2O_3 phase and mullite ($3Al_2O_3 \cdot 2SiO_2$) to an X-ray amorphous phase. The use of a complex electrolyte leads to a two-phase state of the coating with a large (compared to an alkaline electrolyte) shift of the γ–$Al_2O_3 \rightarrow \alpha$–$Al_2O_3$ transformation towards the formation of the α–Al_2O_3 phase. It was determined that the value of hardness correlates with the content of the α–Al_2O_3 phase in the MAO coating, reaching the maximum value of 1620 kg/mm^2 at the highest content (about 80 vol. %) of the α–Al_2O_3 phase.

Two types of dependences of the coating thickness on the amount of electricity passed were revealed. For the amount of passed electricity 10–50 A-h/dm^2, the thickness dependence is determined as 4.2 μm/(A-h/dm^2), which suggests the basic mechanism of electrochemical oxidation during the formation of a coating. For the amount of electricity transmitted 50–120 A-hour/dm^2, the thickness dependence is determined by a much smaller value of 1.1 μm/(A-hour/dm^2). This suggests a transition to a different mechanism of coating formation – the formation of a coating with the participation of electrolysis components

Keywords: structural engineering, microarc oxidation, D16 alloy, electrolyte type, growth kinetics, phase composition

UDC 539.216.2: 537.52
DOI: 10.15587/1729-4061.2020.209722

A STUDY OF THE PHASE-STRUCTURAL ENGINEERING POSSIBILITIES OF COATINGS ON D16 ALLOY DURING MICRO-ARC OXIDATION IN ELECTROLYTES OF DIFFERENT TYPES

V. Subbotina
PhD, Associate Professor*
E-mail: subbotina.valeri@gmail.com
O. Sobol
Doctor of Physics and Mathematics Sciences, Professor*
E-mail: sool@kpi.kharkov.ua
V. Belozerov
PhD, Professor*
E-mail: belozerov.valerii@gmail.com
A. Subbotin
Researcher*
E-mail: subbotin.alex95@gmail.com
Yu. Smyrnova
PhD, Associate Professor
Department of Chemistry and Integrated Technologies
O.M. Beketov National University
of Urban Economy in Kharkiv
Marshala Bazhanova str., 17, Kharkiv, Ukraine, 61002
E-mail: Yuliia.Smyrnova@kname.edu.ua
*Department of Materials Science
National Technical University „Kharkiv Polytechnic Institute“
Kyrpychova str., 2, Kharkiv, Ukraine, 61002

Received date 06.07.2020
Accepted date 24.07.2020
Published date 31.08.2020

1. Introduction

Coatings are the basis of most modern technologies in mechanical engineering, aircraft construction and medical technology [1, 2]. The most promising directions in the field of creating multifunctional coatings are multi-element [3, 4], multilayer [5, 6] and hybrid (formed from a base material with a partial thickness increment [7, 8]) coatings. In recent years, the method of structural engineering of coatings has been effectively used to form coatings with desired properties [9, 10].

The method of structural engineering of coatings (i. e., determination of regularities of structural states depending on the parameters of obtaining coatings) has gained especially great importance due to the use of highly nonequilibrium methods of their formation from plasma [11, 12].

Among the most promising technologies in this direction is low-temperature plasma treatment of valve materials

(Al, Ti, Mg, Nb, Zr, etc.), which transforms surface layers into oxide ceramic coatings [13, 14]. This process was originally called plasma electrolytic oxidation (PEO) [15, 16], and somewhat later – anodic spark deposition (ASD) [17]. However, the most frequently used name recently in describing this process is microarc oxidation (MAO) [18, 19]. As a result of the MAO process, coatings with a thickness of 100–300 μm are formed on the surface with a unique combination of physical and mechanical properties (high hardness, wear resistance, heat resistance, heat strength, corrosion resistance, etc.) [20, 21].

Therefore, at present, the industrial implementation of this technology is very promising, and the development of the method of structural engineering to achieve the required properties in coatings of this type is an urgent and demanded task.

2. Literature review and problem statement

As shown in [22, 23], there is a fundamental difference between anodizing and microarc oxidation. Unlike anodizing, where oxidation does not occur by continuous transfer of ions through the electrolyte (in a thin oxide layer), in microarc oxidation, oxidation occurs due to the combination of metal and oxygen atoms (or ions) in the discharge plasma. This mechanism facilitates the production of thicker oxide layers and often results in a harder and larger crystallite structure. The main reason for this is that the discharges generate a large amount of heat, which promotes crystallization in the surrounding oxide material [24, 25]. In this case, during the MAO treatment, there is no significant increase in the substrate temperature [26, 27].

A specific feature of the MAO process is the use of valve materials on which oxide films (formed electrochemically) have unipolar or asymmetric conductivity in the metal – oxide – electrolyte (MOE) system [28, 29]. In this case, the positive potential on the metal (on which the anodic oxide film is formed) corresponds to the blocking or reverse direction, i. e., the system works similarly to a semiconductor valve.

Thus, MAO is simultaneously characterized by the features of two different groups of modification methods: coating deposition (with an increment in thickness) and changes in the structure and properties of the surface and near-surface layers (without an increment in thickness) [30, 31].

Using this method, the highest properties have now been obtained on aluminum alloys [32, 33]. This is associated with the possibility of the formation of a highly hard α–Al_2O_3 phase during the MAO process [34, 35].

However, the mechanism of the formation of this phase, due to the complexity and heterogeneity of the MAO process, cannot yet be theoretically predicted. Therefore, to determine the patterns and mechanisms of the formation of the phase-structural state in the MAO process, empirical data are currently used for different technological conditions [36, 37]. In this case, as a rule, the phase composition of the coatings changes over the MAO layer thickness [38, 39]. During MAO processing of alloys based on aluminum, it was found that high-temperature modifications of aluminum oxide are in its inner layers. Towards the outer surface of the modified layer, the amount of low-temperature modifications of aluminum oxide increases. It is assumed that the latter is associated with the conditions of electrolysis at the initial stages of anode-spark treatment, since the temperature of the metal sections adjacent to the discharge craters is only 400–500 °C [40].

Also, a very important factor in the MAO treatment is the type and number of impurity atoms. Usually, metals with a high free energy of oxide formation are used as impurity atoms [41]. However, in many cases, aluminum alloys with other alloying elements are used to achieve the required performance characteristics. In particular, the main alloying element of the widely used D16 alloy (and its analogs) is copper, which has low oxidation energy. The effect of such a combination of elements can lead to specific features of the kinetics of the growth of coatings and their phase-structural formation [42, 43]. For this type of alloy (D16), it is known to use aqueous solutions based on sodium hydroxide (NaOH) as electrolytes [44]. Studies of MAO coatings with an alkaline constituent of NaOH electrolyte have shown that even in a complex electrolyte ($NaOH+Na_2SiO_3$), their growth kinetics is relatively low (the growth rate at a thickness of more than 100 μm does not exceed 0.5 μm/min) [44]. The proportion of the hardest α-Al_2O_3 phase does not exceed 70 vol. %. Since the stability of the electrolyte requires an alkaline medium with a high pH (hydrogen index), an increase in the kinetics of coating growth can be expected when using potassium hydroxide (with a higher pH=13) as an alkaline electrolyte component [41].

Therefore, for electrolysis in alkaline electrolytes, it is important, both from a scientific and a practical point of view, to determine the regularities necessary for the phase-structural engineering of MAO coatings. As follows from [41], such regularities should be based on the influence of the type and composition of electrolytes and treatment modes on the kinetics of MAO coatings growth, the quantitative ratio of different phases and their structural states in them.

3. The aim and objectives of the study

The aim of the study was to examine the effect of the type (KOH, Na_2SiO_3 and $KOH+Na_2SiO_3$ solutions) and composition of the electrolyte on the growth kinetics of MAO coatings on the D16 alloy, the formation of their phase-structural state, and the effect of the phase composition on hardness.

To achieve this goal, the following objectives were set:

– to study the effect of the compositions of alkaline (KOH solutions) and silicate (Na_2SiO_3 solutions) electrolytes on the growth kinetics and phase composition of MAO coatings;

– to determine the growth kinetics of MAO coatings formed in a complex ($KOH+Na_2SiO_3$ solutions) electrolyte;

– to study the effect of the complex ($KOH+Na_2SiO_3$ solutions) electrolyte on the formation of the structural-phase state and the hardness of MAO coatings, as well as the electrolysis conditions (the amount of electricity passed) in the electrolyte of this type on the thickness of the formed coatings.

4. Material and technique for studying the effect of the type and composition of electrolyte on the structure and properties of MAO coatings

Samples made of the D16 aluminum alloy were subjected to MAO treatment (composition of the main elements Al (90.9–94.7 %), Cu (3.8–4.9 %), Mg (1.2–1.8 %), Mn – in the range of 0.3–0.9 %, Fe – no more than 0.5 %; Si – no more than 0.5 %; Zn – up to 0.25 %; Ti – no more than 0.15 %. The

samples were in the form of cylinders 30 mm in diameter and 10 mm in height.

Since the MAO process does not require specialized surface treatment (for example, etching or degreasing), the preliminary surface treatment before MAO treatment was only grinding of surface irregularities on abrasive paper.

Microarc oxidation was carried out in a 100-liter bath. During the MAO process, cooling and bubbling of the electrolyte were provided. The average voltage was 380 V. The initial current density was 20 A/dm^2, the duration of treatment was varied.

The following electrolytes were used:

1) alkaline (potassium hydroxide (KOH) solution in distilled water) or silicate (with different percentages of Na_2SiO_3) electrolytes;

2) complex electrolytes (KOH – 1 g/L+Na_2SiO_3 – 3 g/L and KOH – 1 g/L+Na_2SiO_3 – 6 g/L).

A typical microstructure of the lateral section of the near-surface layer of the alloy after MAO treatment is shown in Fig. 1.

One can see the formation, which is standard for the MAO process of aluminum alloys, in addition to the hard base layer of a technological surface layer with low hardness [44]. The technological surface layer (usually with a thickness of 30–40 % of the base layer) with low hardness after the MAO process was removed by the standard grinding method [44].

Therefore, the results obtained in this work refer to the main (base) coating layer.

The determination of the phase composition of MAO coatings was carried out according to the results of X-ray phase analysis. The studies were carried out on a DRON-3 setup (Burevesnik, Russia) in monochromatic K_α–Cu radiation. Diffraction spectra were recorded using the Bragg-Brentano reflection scheme [45]. The survey was carried out both in continuous and pointwise mode with a step of 2θ=0.1°. The maximum error in determining the content of structural crystalline components (with a detectability of 10 vol. %) does not exceed ±0.7 %. The minimum detectability of structural components is about 1 vol. %. This detection accuracy was determined by comparing the reference lines of the phases with the base mixtures.

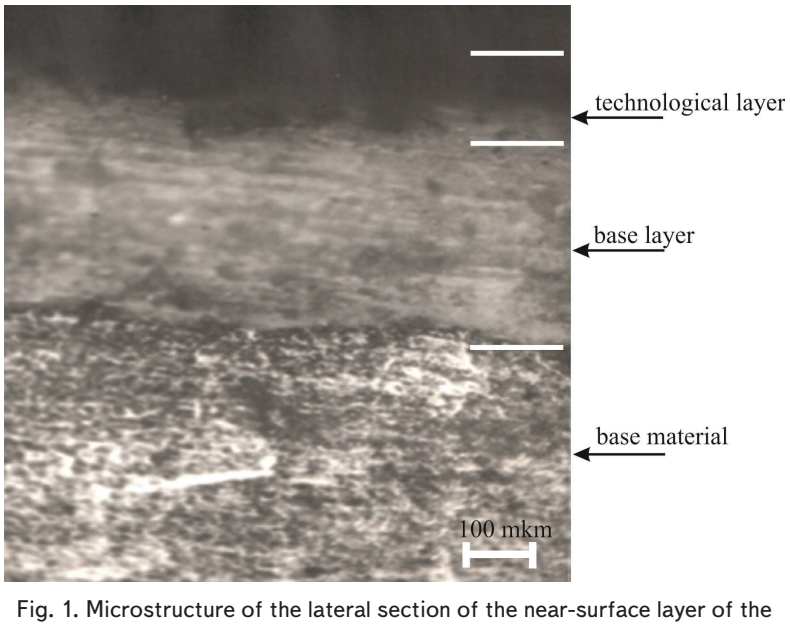

Fig. 1. Microstructure of the lateral section of the near-surface layer of the alloy after MAO treatment

For quantitative phase analysis, the method of reference mixtures was used [46]. For this, calibration graphs of the dependence of the intensities of the comparison lines on the mixture composition were constructed. A–Al_2O_3 (ASTM Card File 10-173), γ–Al_2O_3 (ASTM Card File 10-425) and mullite ($3Al_2O_3{\cdot}2SiO_2$, ASTM Card File 15-776) were used as the basic components of the coating composition. If peaks from the aluminum substrate appeared in the diffraction spectra, they were not taken into account when calculating the coating composition.

The coating thickness was determined on a VT-10 NTs vortex thickness gauge (Kontrolpribor, Russia). The error in measuring the coating thickness is no more than 5 % at the smallest coating thickness (about 10 microns). With a larger coating thickness, the accuracy of determining the thickness increases (for example, at a thickness of 50 μm, the measurement error is no more than 2 %).

The thickness of the layers on the VT-10 NTs device was determined sequentially: first, as complete (base and technological layer), and after grinding the technological layer, the thickness of the base layer was determined.

To determine the amount of electricity Q passed through, the product of current and processing time was used.

Microhardness was determined on a PMT-3 device (LOMO AO, Russia).

5. Results of studying the growth kinetics and phase-structural state of MAO coatings on D16 alloy

5. 1. Growth kinetics and phase composition of MAO coatings during oxidation in alkaline and silicate electrolytes

An alkaline electrolyte is a solution of caustic potassium (KOH) in distilled water, and a silicate electrolyte is an aqueous solution of sodium (Na_2SiO_3) or potassium (K_2SiO_3) water glass.

The introduction of alkali into the electrolyte significantly reduces the outer technological layer. In this case, one of the main factors for the effective use of alkaline electrolyte is the growth kinetics of the coating.

Fig. 2 shows the dependences of the thickness of the coatings on the D16 alloy for different KOH contents in the alkaline electrolyte.

It is seen that with an increase in the KOH content, the growth rate of the coating on the D16 alloy increases. Based on the obtained dependences, the kinetic factor (coating growth rate V) varies from $V_{1\,g/L\text{-}KOH}$= =0.33 μm/min and $V_{2\,g/L\text{-}KOH}$=0.83 μm/min to $V_{5g/L\text{-}KOH}$=1.33 μm/min. Thus, with an increase in the KOH content in the electrolyte from 1 g/L KOH to 5 g/L KOH, the growth rate of the coating increases by more than 4 times.

However, the use of the 5 g/L KOH content is apparently the highest for the process with the formation of microarc discharges. As was found experimentally, at a higher KOH content in the electrolyte, the oxidation process in the microarc discharge mode does not occur, which does not allow the MAO coating to grow (accordingly, at a higher KOH content, there is no possibility of plotting kinetic

dependences in Fig. 2). The reason for this may be the formation of a relatively thick dielectric layer on the growth surface, for which the breakdown voltage significantly exceeds the characteristics in a microarc discharge.

The regularities of the formation of the phase composition and structure that are formed in MAO coatings are the basis for the scientific substantiation and use of the method of phase-structural engineering.

Fig. 3 shows a typical X-ray diffraction spectrum of an MAO coating on the D16 alloy in an alkaline electrolyte.

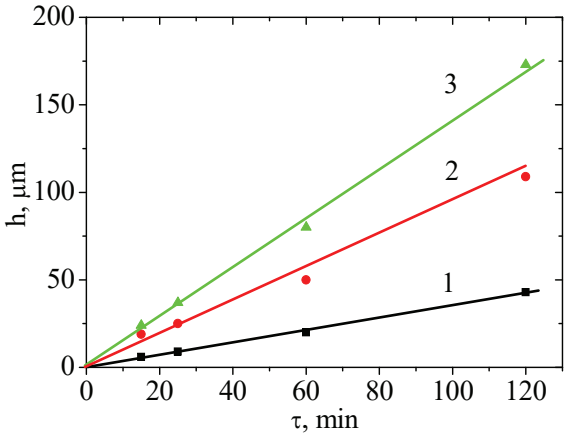

Fig. 2. Kinetics of the formation of coating thickness on the D16 alloy in alkaline electrolytes: 1 – 1 g/L KOH; 2 – 2 g/L KOH; 3 – 5 g/L KOH

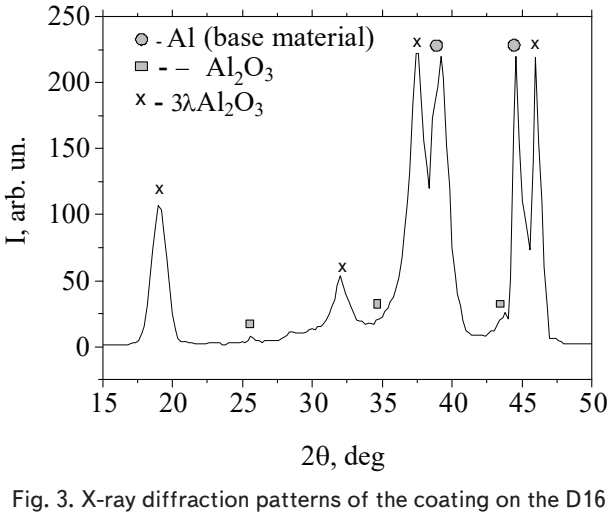

Fig. 3. X-ray diffraction patterns of the coating on the D16 alloy (K_α–Cu radiation, electrolyte – 2 g/L KOH)

It is seen that the main component of the coating is γ–Al_2O_3. Diffraction peaks of the base material (aluminum) are detected by the presence of sample anchorage points, at which oxidation did not occur. In addition to γ–Al_2O_3, diffraction peaks from the α–Al_2O_3 phase (corundum) are revealed in the diffraction spectra. This indicates the presence of crystallites of this phase in the coating.

The dependence of the change in the phase composition on the KOH content in the electrolyte is shown in Fig. 4, *a*. As can be seen from the data obtained, the coating formation process begins with the formation of the γ–Al_2O_3 phase. An increase in the processing time leads to the appearance of α–Al_2O_3 as a result of the thermodynamically favorable polymorphic transformation γ–$Al_2O_3 \rightarrow \alpha$–$Al_2O_3$ [47]. It can be seen that with an increase in the KOH content, the ratio of the volumetric content of γ–Al_2O_3 and α–Al_2O_3 phases changes towards a relative increase in the α–Al_2O_3 phase.

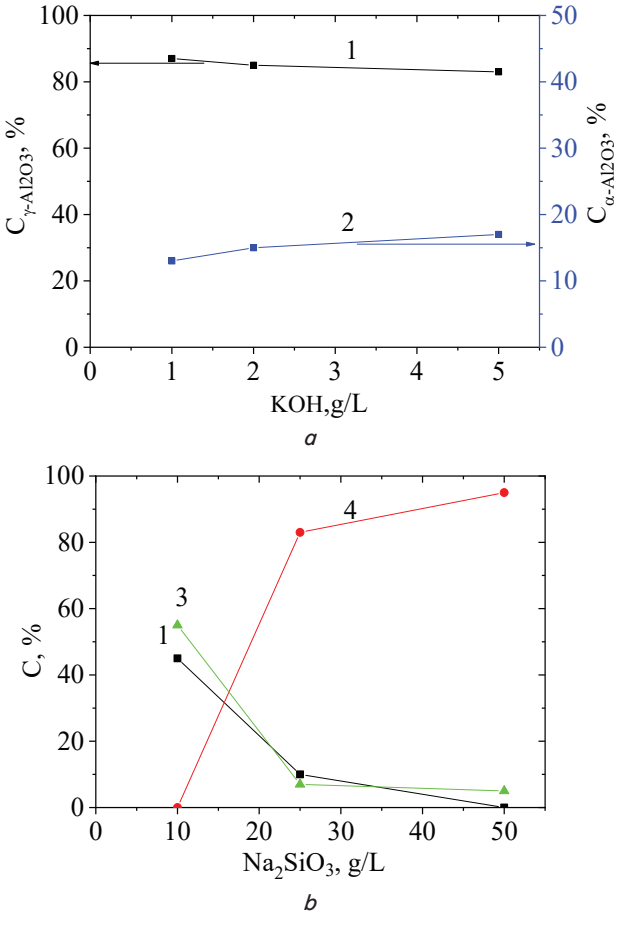

Fig. 4. Phase composition of coatings during their formation in: *a* – alkaline (KOH); *b* – silicate (Na_2SiO_3) electrolytes with different contents (formation time 60 minutes); 1 – γ–Al_2O_3; 2 – α–Al_2O_3; 3 – $3Al_2O_3 \cdot 2SiO_2$ (mullite); 4 – X-ray amorphous phase

This effect is explained by an increase in the relative thickness of the dielectric layer with an increase in the KOH content in the electrolyte. With an increase in the thickness of such a layer, the power of microarc discharges (and, accordingly, the temperature of the microarc process) increases, which stimulates an increase in the completeness of the polymorphic transformation γ–$Al_2O_3 \rightarrow \alpha$–$Al_2O_3$.

An increase in the time of microarc oxidation leads to a further change in the α–Al_2O_3/γ–Al_2O_3 ratio. Fig. 5 shows the dependences of the phase ratio with increased duration of micro-arc oxidation by 3 times (up to 180 minutes).

Fig. 5 shows that an increase in the duration of the MAO process over 60 minutes leads to a significant increase in the relative content of the hardest α–Al_2O_3 phase in the MAO coating. In this case, as can be seen from Fig. 2, the thickness of such coatings reaches 170 μm.

The second, promising from the point of view of technology and ecology of obtaining a coating, is an aqueous solution of sodium or potassium liquid glass [33].

To study the possibilities of phase-structural engineering of MAO coatings on the D16 alloy, we used sodium liquid glass Na_2SiO_3 (GOST 13078-81). Thus, a silicate electrolyte was obtained, the concentration of Na_2SiO_3 in which varied in the range of 10–50 g/L.

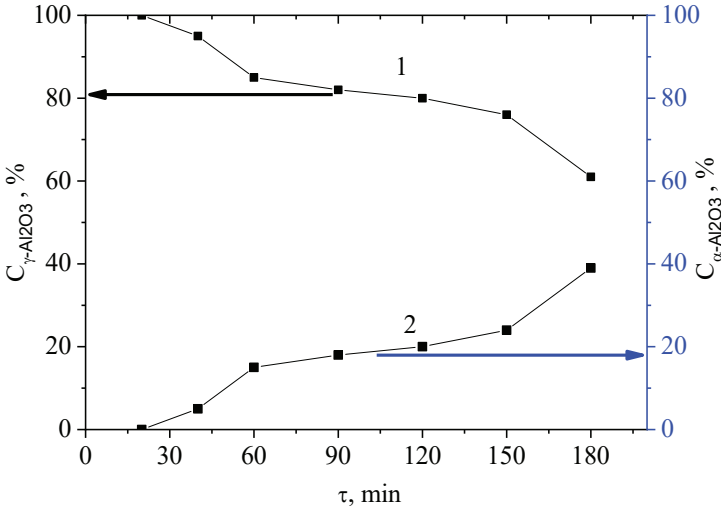

Fig. 5. Phase composition of coatings obtained in an alkaline electrolyte (with 5 g/L KOH): 1 – γ–Al_2O_3; 2 – α–Al_2O_3

The growth kinetics of the coating, determined from its thickness, is shown in Fig. 6. It can be seen that for the composition of the silicate electrolyte with 10 g/L Na_2SiO_3, the growth rate $V_{10\ g/L\text{-}Na2SiO3}$=1.08 μm/min. An increase in the content of water glass in the electrolyte to 25 g/L Na_2SiO_3 leads to a significant increase in the growth rate of the coating up to $V_{25\ g/L\text{-}Na2SiO3}$=2.25 μm/min. The highest growth rate of the coating ($V_{50\ g/L\text{-}Na2SiO3}$=8 μm/min) was achieved when the electrolyte contained 50 g/L Na_2SiO_3 (Fig. 6).

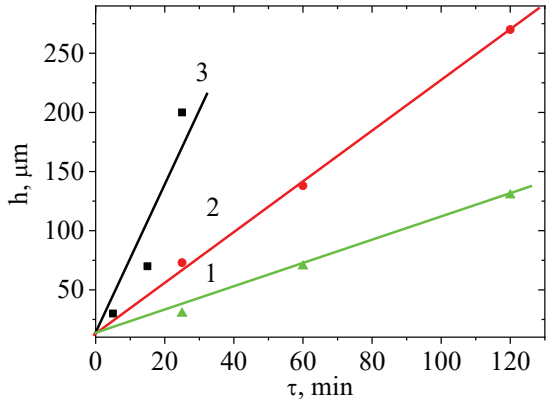

Fig. 6. Kinetics of coating thickness formation on the D16 alloy in silicate electrolyte: 1 – 10 g/L Na_2SiO_3; 2 – 25 g/L Na_2SiO_3; 3 – 50 g/L Na_2SiO_3

It can also be noted that in order to achieve a thickness of 100 μm (used for comparison), depending on the amount of liquid glass, there is a significant change in the time of the MAO process. With a relatively small content of 10 g/L Na_2SiO_3 (Fig. 6, dependence 1), to achieve a working thickness of 100 μm, it is necessary to carry out the MAO process for 120 minutes. In an electrolyte containing 25 g/L Na_2SiO_3, 47 minutes of the MAO process is enough to reach a thickness of 100 μm. Note that at the highest Na_2SiO_3 content of 50 g/L, it takes only 15 minutes to achieve an MAO coating thickness of 100 μm.

As seen from Fig. 7, the typical form of the X-ray diffraction patterns is characterized by the formation of mainly mullite ($3Al_2O_3{\cdot}2SiO_2$), γ–Al_2O_3, and an amorphous-like phase. An increase in the duration of the process for a silicate electrolyte mainly leads to an increase in the content of the X-ray amorphous phase (Fig. 4, *b*). Thus, in the silicate electrolyte there is a significant decrease in the size of the regions of formation and the transition from the crystalline structure of the coating to nanodispersed (X-ray amorphous).

The generalized dependences of the change in the phase composition on the content of water glass are shown in Fig. 4, *b*. It can be seen that only at a relatively low content of liquid glass (10 g/L Na_2SiO_3), the two-phase state from γ–Al_2O_3 and $3Al_2O_3{\cdot}2SiO_2$ (mullite) phases is achieved. Moreover, as follows from Fig. 6, the deposition rate of such a coating is $V_{10\ g/L\text{-}Na2SiO3}$=1.08 μm/min. If compared with the data in Fig. 2, 4, *a* for an alkaline electrolyte KOH, at its highest content of 5 g/L, the two-phase state is also formed, but at a higher growth rate $V_{5g/L\text{-}KOH}$= =1.33 μm/min. However, not only the growth rate is higher, but most importantly, the second phase is not $3Al_2O_3{\cdot}2SiO_2$ (mullite) (as in silicate electrolyte), but the hardest α–Al_2O_3 (corundum).

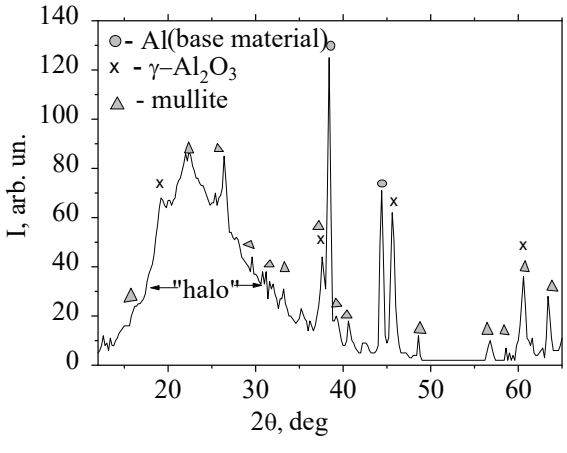

Fig. 7. X-ray diffraction patterns of the coating on the D16 alloy (Kα – Cu radiation, electrolyte – 25 g/L Na_2SiO_3, τ=120 min)

5. 2. Growth kinetics of MAO coatings during oxidation in a complex electrolyte

The results of studying coatings in an alkali-silicate electrolyte are shown in Fig. 8–12. The results refer to the main hardened layer (the process layer is removed).

The dependence of the coating thickness on the oxidation time for two compositions of complex electrolytes is shown in Fig. 8. Treatment was carried out in electrolytes of the compositions KOH (1 g/L)+Na_2SiO_3 (3 g/L) (dependence 1) and KOH (1 g/L)+Na_2SiO_3 (6 g/L) (dependence 2) at a current density j=20 A/dm^2. As can be seen from the data obtained, the kinetics of the formation of the coating thickness depends on the composition. In this case, the growth rate varies from $V_{1\ g/L\text{-}KOH+3g/L\text{-}Na2SiO3}$=0.875 μm/min to $V_{1\ g/L\text{-}KOH+6g/L\text{-}Na2SiO3}$=1.25 μm/min. Thus, the growth rate is within the optimal range for the formation of crystalline γ–Al_2O_3 and α–Al_2O_3 phases (Fig. 1, 5).

The linearity of the obtained dependence indicates that the thickness of the coating is proportional to the deposition time, and, accordingly, to the amount of electricity passed. In this case, as it was found experimentally, with a higher filling of the complex electrolyte with an alkaline or silicate component, the MAO treatment process turns into an arc

one, which manifests itself in the form of cracks and leads to the destruction of the coating [41].

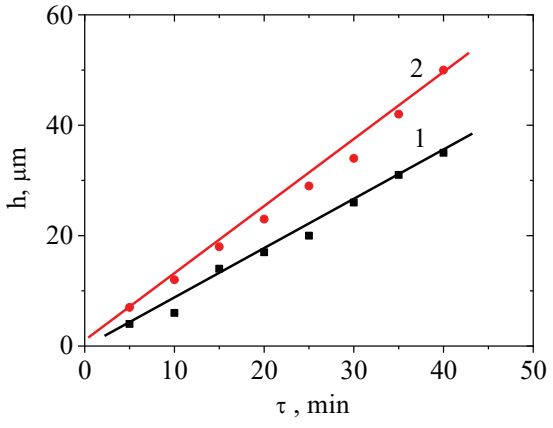

Fig. 8. Kinetics of MAO coating formation: 1 – in an electrolyte with the composition KOH (1 g/L)+ +Na_2SiO_3 (3 g/L); 2 – in an electrolyte with the composition KOH (1 g/L)+Na_2SiO_3 (6 g/L)

Thus, it can be concluded that electrolyte compositions providing a growth rate of 1.2–1.3 μm/min lead to the formation of crystalline γ–Al_2O_3 and α–Al_2O_3 phases with the highest properties.

Due to the higher growth kinetics, electrolysis in an electrolyte with the composition KOH (1 g/L)+Na_2SiO_3 (6 g/L) was used as a base for further studies.

5. 3. Phase composition and properties of MAO coatings during oxidation in a complex electrolyte

X-ray diffraction phase-structural analysis showed that the coatings obtained by microarc oxidation in an electrolyte with the composition KOH (1 g/L)+Na_2SiO_3 (6 g/L) have a crystalline structure (Fig. 9). The main phases of the coating are the γ–Al_2O_3 and α–Al_2O_3 phases. The presence of a spectrum of peaks with a standard intensity from the planes of the crystalline phases indicates the absence of their preferred orientation (texture). The predominant phase at the beginning of the MAO process (at a small coating thickness) is γ–Al_2O_3. With an increase in the time of the MAO process and an increase in the coating thickness, a more complete polymorphic transformation γ–Al_2O_3→α–Al_2O_3 occurs (Fig. 10).

Thus, as follows from the results shown in Fig. 10, in order to increase the content of the α–Al_2O_3 phase in the MAO coating to 50 %, it is necessary to form a coating with a thickness of more than 100 μm. At a thickness of about 240 μm, the relative content of the α–Al_2O_3 phase reaches 84 vol. %.

A change in the content of the α–Al_2O_3 phase leads to a change in the hardness of the coatings (Fig. 11). In this case, a proportional increase in the hardness of the coating with an increase in the content of the α–Al_2O_3 phase is observed.

Oxidation of the D16 alloy at different current densities (12–23 A/dm^2) showed that the thickness of the coating is determined by the amount of electricity passed, defined in A-hour/dm^2 (Fig. 12).

As seen from Fig. 12, the dependence of the coating thickness on the amount of transmitted electricity has two characteristic areas. The first section is in the range of 10–50 A-h/dm^2, and the second – in the range of 50–120 A-h/dm^2.

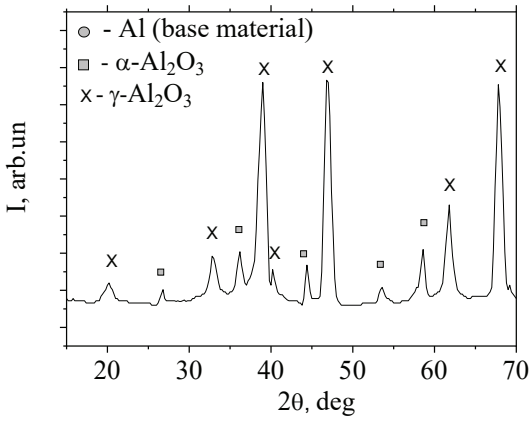

Fig. 9. X-ray diffraction patterns of the coating on the D16 alloy (K_α – Cu radiation, electrolyte KOH (1 g/L)+ +Na_2SiO_3 (6 g/L), τ=45 minutes)

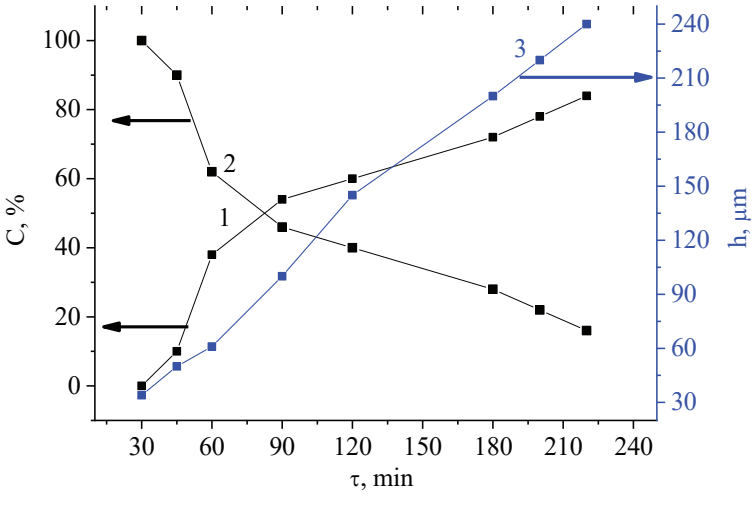

Fig. 10. Phase composition and thickness of coatings obtained in a complex electrolyte KOH (1 g/L)+Na_2SiO_3 (6 g/L): 1 – α–Al_2O_3; 2 – γ–Al_2O_3, 3 – coating thickness

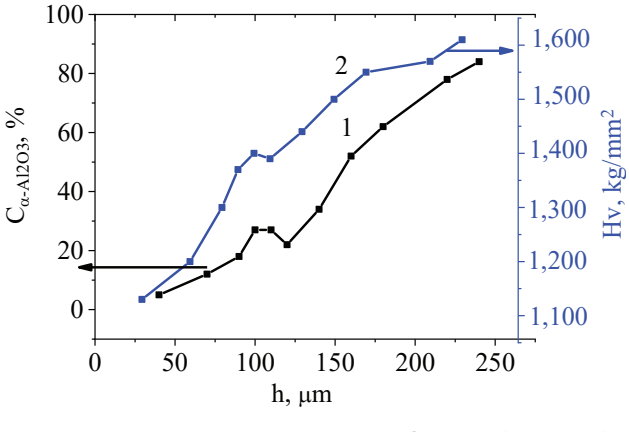

Fig. 11. Volumetric content of the α–Al_2O_3 phase (corundum) (1) and microhardness of the main (working) coating layer depending on the coating thickness (D16 alloy, KOH electrolyte (1 g/L)+Na_2SiO_3 (6 g/L), current density 10–20 A/dm^2)

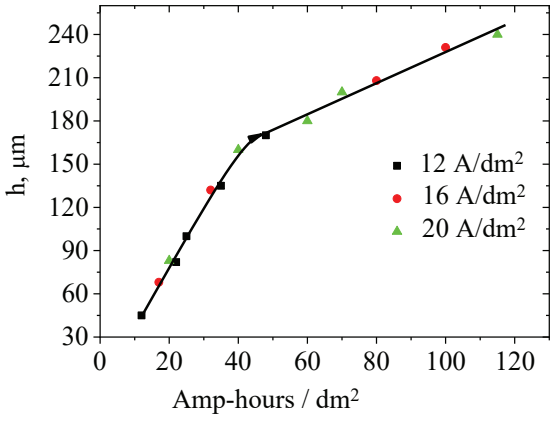

Fig. 12. Influence of the amount of electricity passed (Ampere-hour per dm^2) on the coating thickness, h (D16 alloy, electrolyte 1 g/L KOH+6 g/L Na_2SiO_3)

6. Discussion of the results of the influence of different types of electrolytes on the growth kinetics, phase-structural state and properties of MAO coatings

An analysis of the results obtained indicates that the choice of the type of electrolyte and the conditions for the process of microarc oxidation can significantly change the phase-structural state and surface properties of the D16 aluminum alloy. The use of an alkaline electrolyte (KOH) allows a significant increase in the power of microarc discharges, which contributes to the formation of the hardest α–Al_2O_3 phase (Fig. 3, 4, *a*). This is a consequence of the completeness of the γ–$Al_2O_3 \rightarrow \alpha$–$Al_2O_3$ polymorphic transformation during the formation of coatings. In this case, the composition of the coating changes to the greatest extent with an increase in the duration of the process, reaching, with a duration of 180 min, compositions of 60 vol. % γ–Al_2O_3 – 40 vol. % α–Al_2O_3 (Fig. 5). The kinetics of the formation of such coatings increases with an increase in the KOH content in the electrolyte (Fig. 3). However, there is a limitation on the percentage of KOH content associated with the conditions for the formation of micro-arc discharges. It was found that an increase in the KOH content of more than 5 g/L does not ensure the implementation of the process in the mode of microarc discharges, which does not allow the formation of MAO coatings on the D16 alloy.

It should also be noted that the early results obtained for the AMg6 alloy, where Mg was the main alloying element (up to 5.8 %), showed that the γ–$Al_2O_3 \rightarrow \alpha$–$Al_2O_3$ transformation did not occur at all under similar conditions [48]. Thus, alloying of aluminum with copper is an important factor for the γ–$Al_2O_3 \rightarrow \alpha$–$Al_2O_3$ transformation. Although, in comparison with the AMg6 alloy, the rate of formation of the coating on the D16 alloy decreases. One of the reasons determining the noted features, apparently, is the low oxidizing ability of copper. However, to determine the mechanisms of such an effect, additional studies of the MAO process in alloys with different elemental compositions are required.

When using liquid glass (Na_2SiO_3) as an electrolyte filler, the growth kinetics of the MAO coating increases (Fig. 6). However, an increase in the growth rate of the coating is accompanied in the silicate electrolyte by a decrease in the formation voltage, which leads to the formation of phases with a low density (mullite ($3Al_2O_3{\cdot}2SiO_2$) and an amorphous-like phase, Fig. 4, *b*, 7).

The use of a complex alkali-silicate electrolyte allows, at a relatively low content (1 g/L KOH+6 g/L Na_2SiO_3), forming a two-phase coating (γ–Al_2O_3 and α–Al_2O_3) at a relatively high growth rate of 1.25 μm/min (Fig. 8–10). At the same time, an increase in the duration of the process also makes it possible to increase the relative content of the α–Al_2O_3 phase in the coating (Fig. 10). The hardness of such coatings increases with an increase in the content of the α–Al_2O_3 phase and reaches 1,620 kg/mm^2 at a content of about 80 vol. % α–Al_2O_3 phase (Fig. 11).

The dependence of the coating thickness on the amount of passed electricity has two characteristic areas (Fig. 12), which indicates two mechanisms of coating formation. The first of these mechanisms is manifested in the 10–50 A-hour/dm^2 section. As can be seen from the data obtained, in this area the dependence has an average ratio of 4.2 μm/(A-hour/dm^2). Such a large ratio of the coating thickness to the transmitted electricity is determined by the main mechanism in MAO treatment – the formation of a coating by the mechanism of electrochemical oxidation. In the second characteristic section, 50–120 A-hour/dm^2, the average ratio of the coating thickness to the amount of passed electricity decreases to 1.1 μm/(A-hour/dm^2). The most probable reason for this decrease is the transition to a different mechanism of coating formation – the formation of a coating with the participation of electrolysis components. It is known that the formation of oxide as a result of deposition from the electrolyte leads to loose and poorly bonded coatings [49, 50].

Thus, for an aluminum-based alloy with a copper content of about 4 wt. %, the use of an alkaline (KOH) electrolyte allows the formation of a two-phase (γ–Al_2O_3 and α–Al_2O_3) state. In this case, as the duration of the process increases, the relative content of the α–Al_2O_3 phase increases. The use of a complex electrolyte makes it possible to increase the growth rate of such a coating and to a greater extent to proceed the reactions of the polymorphic transformation γ–$Al_2O_3 \rightarrow \alpha$–$Al_2O_3$.

Thus, the results obtained can be used to improve the functional properties of aluminum alloys of the D16 type (an aluminum alloy with a copper content of about 4 wt. %). As follows from a comparison with the results obtained on the microarc oxidation of the AMg6 alloy [48], the use of other elements for alloying can significantly change the formation kinetics of the MAO coating and its phase composition. Therefore, in order to establish universal regularities for different types of aluminum alloys, further studies are required, which imply the determination of regularities in the structural-phase transformations of MAO coatings on aluminum alloys with metals, for which the oxidation energy is higher than for copper (V, Nb, Ta, and Cr).

7. Conclusions

1. It was found that for alkaline (KOH solutions) and silicate (Na_2SiO_3 solutions) electrolytes, with an increase in the content of components, the growth rate of MAO coatings increases. With an increase in the KOH content from 1 g/L to 5 g/L, the growth rate of the coating increases from 0.33 to 1.33 μm/min. With an increase in the content of liquid glass from 10 g/L Na_2SiO_3 to 50 g/L Na_2SiO_3, the growth rate increases from 1.08 to 2.25 μm/min. It was revealed that the phase composition of MAO coatings formed on the D16 alloy in alkaline (KOH) electrolyte consists of γ–Al_2O_3 and α–Al_2O_3 phases. An increase in the KOH concentration leads to a shift in the γ–$Al_2O_3 \rightarrow \alpha$–$Al_2O_3$ polymorphic trans-

formation towards the formation of the hardest α–Al_2O_3 phase (corundum). The addition of liquid glass (Na_2SiO_3) in the electrolyte composition significantly increases the growth rate of the coating; however, the size of the ordering regions decreases from crystalline to X-ray amorphous.

2. It was determined that in a complex alkaline-silicate (KOH+Na_2SiO_3 solutions) electrolyte, a growth rate of about 1 μm/min is achieved at a lower relative content of components. It was found that with an alkaline component (KOH) of 1 g/L and an increase in the silicate (Na_2SiO_3) component of 3 g/L to 6 g/L, the growth rate of the MAO coating increases from 0.875 μm/min to 1.25 μm/min.

3. It is shown that the use of a complex alkaline-silicate electrolyte leads to a two-phase state of the coating with a large (compared to alkaline electrolyte) shift of the γ–Al_2O_3→α–Al_2O_3 transformation towards the formation of the α–Al_2O_3 phase. It was found that the value of the hardness of such coatings correlates with the content of the α–Al_2O_3 phase in the MAO coating, reaching the highest value of 1620 kg/mm^2 at the highest content (about 80 vol. %) of the α–Al_2O_3 phase. For MAO coatings obtained in a complex alkali-silicate electrolyte, two types of dependences of the coating thickness on the amount of electricity passed were revealed. For the amount of electricity passed 10–50 A-h/dm^2, the thickness dependence is determined as 4.2 μm/(A-h/dm^2), which suggests the basic mechanism of electrochemical oxidation during the formation of a coating. For the amount of passed electricity 50–120 A-h/dm^2, the thickness dependence is determined by a much lower value of 1.1 μm/(A-h/dm^2), which suggests a transition to a different mechanism of coating formation – the formation of a coating with the participation of electrolysis components.

Acknowledgments

The authors would like to express their gratitude to the Ministry of Education and Science of Ukraine for financial support within the framework of the project "Development of material science bases for the use of high-performance ion-plasma technologies for three-level surface engineering" (state registration No. 0118U002044).

References

1. Smith, J. R., Lamprou, D. A. (2014). Polymer coatings for biomedical applications: a review. Transactions of the IMF, 92 (1), 9–19. doi: https://doi.org/10.1179/0020296713z.000000000157
2. Fedirko, V. M., Pohrelyuk, I. M., Luk'yanenko, O. H., Lavrys', S. M., Kindrachuk, M. V., Dukhota, O. I. et. al. (2018). Thermodiffusion Saturation of the Surface of VT22 Titanium Alloy from a Controlled Oxygen–Nitrogen-Containing Atmosphere in the Stage of Aging. Materials Science, 53 (5), 691–701. doi: https://doi.org/10.1007/s11003-018-0125-z
3. Guo, S., Liu, C. T. (2011). Phase stability in high entropy alloys: Formation of solid-solution phase or amorphous phase. Progress in Natural Science: Materials International, 21 (6), 433–446. doi: https://doi.org/10.1016/s1002-0071(12)60080-x
4. Azarenkov, N. A., Sobol, O. V., Beresnev, V. M., Pogrebnjak, A. D., Kolesnikov, D. A., Turbin, P. V., Toryanik, I. N. (2013). Vacuum-plasma coatings based on the multielement nitrides. Metallofizika i noveishie tekhnologii, 35 (8), 1061–1084. Available at: http://dspace.nbuv.gov.ua/bitstream/handle/123456789/104178/07-Azarenkov.pdf?sequence=1
5. Sobol', O. V., Andreev, A. A., Gorban', V. F. (2016). Structural Engineering of Vacuum-ARC Multiperiod Coatings. Metal Science and Heat Treatment, 58 (1-2), 37–39. doi: https://doi.org/10.1007/s11041-016-9961-3
6. Sobol´, O. V., Andreev, A. A., Gorban´, V. F., Meylekhov, A. A., Postelnyk, H. O. (2016). Structural Engineering of the Vacuum Arc ZrN/CrN Multilayer Coatings. Journal of Nano- and Electronic Physics, 8(1), 01042-1–01042-5. doi: https://doi.org/10.21272/jnep.8(1).01042
7. Xu, F., Xia, Y., Li, G. (2009). The mechanism of PEO process on Al–Si alloys with the bulk primary silicon. Applied Surface Science, 255 (23), 9531–9538. doi: https://doi.org/10.1016/j.apsusc.2009.07.090
8. Belozerov, V., Mahatilova, A., Sobol', O., Subbotina, V., Subbotin, A. (2017). Improvement of energy efficiency in the operation of a thermal reactor with submerged combustion apparatus through the cyclic input of energy. Eastern-European Journal of Enterprise Technologies, 2 (5 (86)), 39–43. doi: https://doi.org/10.15587/1729-4061.2017.96721
9. Sobol, O. V., Postelnyk, A. A., Meylekhov, A. A., Andreev, A. A., Stolbovoy, V. A. (2017). Structural Engineering of the Multilayer Vacuum Arc Nitride Coatings Based on Ti, Cr, Mo and Zr. Journal of Nano- and Electronic Physics, 9 (3), 03003-1–03003-6. doi: https://doi.org/10.21272/jnep.9(3).03003
10. Sobol', O. V., Andreev, A. A., Gorban', V. F., Stolbovoy, V. A., Melekhov, A. A., Postelnyk, A. A. (2016). Possibilities of structural engineering in multilayer vacuum-arc ZrN/CrN coatings by varying the nanolayer thickness and application of a bias potential. Technical Physics, 61 (7), 1060–1063. doi: https://doi.org/10.1134/s1063784216070252
11. Sobol', O. V., Meilekhov, A. A. (2018). Conditions of Attaining a Superhard State at a Critical Thickness of Nanolayers in Multiperiodic Vacuum-Arc Plasma Deposited Nitride Coatings. Technical Physics Letters, 44 (1), 63–66. doi: https://doi.org/10.1134/s1063785018010224
12. Sobol', O. V., Andreev, A. A., Stolbovoi, V. A., Fil'chikov, V. E. (2012). Structural-phase and stressed state of vacuum-arc-deposited nanostructural Mo-N coatings controlled by substrate bias during deposition. Technical Physics Letters, 38 (2), 168–171. doi: https://doi.org/10.1134/s1063785012020307
13. Lesnevskiy, L. N., Lyakhovetskiy, M. A., Ivanova, S. V., Nagovitsyna, O. A. (2016). Structure and properties of surface layers formed on zirconium alloy by microarc oxidation. Journal of Surface Investigation. X-Ray, Synchrotron and Neutron Techniques, 10 (3), 641–647. doi: https://doi.org/10.1134/s1027451016030289
14. Laleh, M., Kargar, F., Sabour Rouhaghdam, A. (2011). Formation of a compact oxide layer on AZ91D magnesium alloy by microarc oxidation via addition of cerium chloride into the MAO electrolyte. Journal of Coatings Technology and Research, 8 (6), 765–771. doi: https://doi.org/10.1007/s11998-011-9357-7

15. Curran, J. A., Clyne, T. W. (2005). Thermo-physical properties of plasma electrolytic oxide coatings on aluminium. Surface and Coatings Technology, 199 (2-3), 168–176. doi: https://doi.org/10.1016/j.surfcoat.2004.09.037
16. Norlin, A., Pan, J., Leygraf, C. (2006). Fabrication of Porous Nb_2O_5 by Plasma Electrolysis Anodization and Electrochemical Characterization of the Oxide. Journal of The Electrochemical Society, 153 (7), B225. doi: https://doi.org/10.1149/1.2196788
17. Curran, J. A., Kalkancı, H., Magurova, Y., Clyne, T. W. (2007). Mullite-rich plasma electrolytic oxide coatings for thermal barrier applications. Surface and Coatings Technology, 201 (21), 8683–8687. doi: https://doi.org/10.1016/j.surfcoat.2006.06.050
18. Li, H. X., Li, W. J., Song, R. G., Ji, Z. G. (2012). Effects of different current densities on properties of MAO coatings embedded with and withoutα-Al2O3nanoadditives. Materials Science and Technology, 28 (5), 565–568. doi: https://doi.org/10.1179/1743284711y.0000000084
19. Veys-Renaux, D., Rocca, E., Henrion, G. (2013). Micro-arc oxidation of AZ91 Mg alloy: An in-situ electrochemical study. Electrochemistry Communications, 31, 42–45. doi: https://doi.org/10.1016/j.elecom.2013.02.023
20. Cui, S., Han, J., Du, Y., Li, W. (2007). Corrosion resistance and wear resistance of plasma electrolytic oxidation coatings on metal matrix composites. Surface and Coatings Technology, 201 (9-11), 5306–5309. doi: https://doi.org/10.1016/j.surfcoat.2006.07.126
21. Chen, J., Wang, Z., Lu, S. (2012). Effects of electric parameters on microstructure and properties of MAO coating fabricated on ZK60 Mg alloy in dual electrolyte. Rare Metals, 31 (2), 172–177. doi: https://doi.org/10.1007/s12598-012-0486-7
22. Mota, R. O., Liu, Y., Mattos, O. R., Skeldon, P., Thompson, G. E. (2008). Influences of ion migration and electric field on the layered anodic films on Al–Mg alloys. Corrosion Science, 50 (5), 1391–1396. doi: https://doi.org/10.1016/j.corsci.2008.01.007
23. Lu, X., Blawert, C., Kainer, K. U., Zheludkevich, M. L. (2016). Investigation of the formation mechanisms of plasma electrolytic oxidation coatings on Mg alloy AM50 using particles. Electrochimica Acta, 196, 680–691. doi: https://doi.org/10.1016/j.electacta.2016.03.042
24. Martin, J., Leone, P., Nominé, A., Veys-Renaux, D., Henrion, G., Belmonte, T. (2015). Influence of electrolyte ageing on the Plasma Electrolytic Oxidation of aluminium. Surface and Coatings Technology, 269, 36–46. doi: https://doi.org/10.1016/j.surfcoat.2014.11.001
25. Jovović, J., Stojadinović, S., Šišović, N. M., Konjević, N. (2011). Spectroscopic characterization of plasma during electrolytic oxidation (PEO) of aluminium. Surface and Coatings Technology, 206 (1), 24–28. doi: https://doi.org/10.1016/j.surfcoat.2011.06.031
26. Gu, W., Shen, D., Wang, Y., Chen, G., Feng, W., Zhang, G. et. al. (2006). Deposition of duplex Al_2O_3/aluminum coatings on steel using a combined technique of arc spraying and plasma electrolytic oxidation. Applied Surface Science, 252 (8), 2927–2932. doi: https://doi.org/10.1016/j.apsusc.2005.04.036
27. Tseng, C.-C., Lee, J.-L., Kuo, T.-H., Kuo, S.-N., Tseng, K.-H. (2012). The influence of sodium tungstate concentration and anodizing conditions on microarc oxidation (MAO) coatings for aluminum alloy. Surface and Coatings Technology, 206 (16), 3437–3443. doi: https://doi.org/10.1016/j.surfcoat.2012.02.002
28. Asadi, S., Kazeminezhad, M. (2016). Multi Directional Forging of 2024 Al Alloy After Different Heat Treatments: Microstructural and Mechanical Behavior. Transactions of the Indian Institute of Metals, 70 (7), 1707–1719. doi: https://doi.org/10.1007/s12666-016-0967-8
29. Yerokhin, A. L., Nie, X., Leyland, A., Matthews, A., Dowey, S. J. (1999). Plasma electrolysis for surface engineering. Surface and Coatings Technology, 122 (2-3), 73–93. doi: https://doi.org/10.1016/s0257-8972(99)00441-7
30. Dunleavy, C. S., Curran, J. A., Clyne, T. W. (2011). Self-similar scaling of discharge events through PEO coatings on aluminium. Surface and Coatings Technology, 206 (6), 1051–1061. doi: https://doi.org/10.1016/j.surfcoat.2011.07.065
31. Matykina, E., Arrabal, R., Pardo, A., Mohedano, M., Mingo, B., Rodríguez, I., González, J. (2014). Energy-efficient PEO process of aluminium alloys. Materials Letters, 127, 13–16. doi: https://doi.org/10.1016/j.matlet.2014.04.077
32. Melhem, A., Henrion, G., Czerwiec, T., Briançon, J. L., Duchanoy, T., Brochard, F., Belmonte, T. (2011). Changes induced by process parameters in oxide layers grown by the PEO process on Al alloys. Surface and Coatings Technology, 205, S133–S136. doi: https://doi.org/10.1016/j.surfcoat.2011.01.046
33. Belozerov, V., Sobol, O., Mahatilova, A., Subbotina, V., Tabaza, T. A., Al-Qawabeha, U. F., Al-Qawabah, S. M. (2017). The influence of the conditions of microplasma processing (microarc oxidation in anodecathode regime) of aluminum alloys on their phase composition. Eastern-European Journal of Enterprise Technologies, 5 (12 (89)), 52–57. doi: https://doi.org/10.15587/1729-4061.2017.112065
34. Subbotina, V., Al-Qawabeha, U. F., Belozerov, V., Sobol, O., Subbotin, A., Tabaza, T. A., Al-Qawabah, S. M. (2019). Determination of influence of electrolyte composition and impurities on the content of α-AL_2O_3 phase in MAO-coatings on aluminum. Eastern-European Journal of Enterprise Technologies, 6 (12 (102)), 6–13. doi: https://doi.org/10.15587/1729-4061.2019.185674
35. Javidi, M., Fadaee, H. (2013). Plasma electrolytic oxidation of 2024-T3 aluminum alloy and investigation on microstructure and wear behavior. Applied Surface Science, 286, 212–219. doi: https://doi.org/10.1016/j.apsusc.2013.09.049
36. Belozerov, V., Sobol, O., Mahatilova, A., Subbotina, V., Tabaza, T. A., Al-Qawabeha, U. F., Al-Qawabah, S. M. (2018). Effect of electrolysis regimes on the structure and properties of coatings on aluminum alloys formed by anodecathode micro arc oxidation. Eastern-European Journal of Enterprise Technologies, 1 (12 (91)), 43–47. doi: https://doi.org/10.15587/1729-4061.2018.121744
37. Subbotina, V. V., Al-Qawabeha, U. F., Sobol', O. V., Belozerov, V. V., Schneider, V. V., Tabaza, T. A., Al-Qawabah, S. M. (2019). Increase of the α-Al_2O_3 phase content in MAO-coating by optimizing the composition of oxidated aluminum alloy. Functional Materials, 26 (4), 752–758. doi: https://doi.org/10.15407/fm26.04.752
38. Friedemann, A. E. R., Gesing, T. M., Plagemann, P. (2017). Electrochemical rutile and anatase formation on PEO surfaces. Surface and Coatings Technology, 315, 139–149. doi: https://doi.org/10.1016/j.surfcoat.2017.01.042
39. Yao, Z., Liu, Y., Xu, Y., Jiang, Z., Wang, F. (2011). Effects of cathode pulse at high frequency on structure and composition of Al_2TiO_5 ceramic coatings on Ti alloy by plasma electrolytic oxidation. Materials Chemistry and Physics, 126 (1-2), 227–231. doi: https://doi.org/10.1016/j.matchemphys.2010.11.035

40. Lv, P. X., Chi, G. X., Wei, D. B., Di, S. C. (2011). Design of Scanning Micro-Arc Oxidation Forming Ceramic Coatings on 2024 Aluminium Alloy. Advanced Materials Research, 189-193, 1296–1300. doi: https://doi.org/10.4028/www.scientific.net/amr.189-193.1296
41. Clyne, T. W., Troughton, S. C. (2018). A review of recent work on discharge characteristics during plasma electrolytic oxidation of various metals. International Materials Reviews, 64 (3), 127–162. doi: https://doi.org/10.1080/09506608.2018.1466492
42. Javidi, M., Fadaee, H. (2013). Plasma electrolytic oxidation of 2024-T3 aluminum alloy and investigation on microstructure and wear behavior. Applied Surface Science, 286, 212–219. doi: https://doi.org/10.1016/j.apsusc.2013.09.049
43. Matykina, E., Arrabal, R., Mohedano, M., Mingo, B., Gonzalez, J., Pardo, A., Merino, M. C. (2017). Recent advances in energy efficient PEO processing of aluminium alloys. Transactions of Nonferrous Metals Society of China, 27 (7), 1439–1454. doi: https://doi.org/10.1016/s1003-6326(17)60166-3
44. Suminov, I. V., Belkin, P. N., Epel'fel'd, A. V., Lyudin, V. B., Krit, B. L., Borisov, A. M. (2011). Plazmenno-elektroliticheskoe modifitsirovanie poverhnosti metallov i splavov. Vol. 2. Moscow: Tekhnosfera, 512.
45. Sobol', O. V., Shovkoplyas, O. A. (2013). On advantages of X-ray schemes with orthogonal diffraction vectors for studying the structural state of ion-plasma coatings. Technical Physics Letters, 39 (6), 536–539. doi: https://doi.org/10.1134/s1063785013060126
46. Klopotov, A. A., Abzaev, Yu. A., Potekaev, A. I., Volokitin, O. G. (2012). Osnovy rentgenostrukturnogo analiza v materialovedenii. Tomsk: Izd-vo Tom. gos. arhit.-stroit. Un-ta, 276.
47. Subbotina, V. V., Sobol, O. V., Belozerov, V. V., Makhatilova, A. I., Shnayder, V. V. (2019). Use of the Method of Micro-arc Plasma Oxidation to Increase the Antifriction Properties of the Titanium Alloy Surface. Journal of Nano- and Electronic Physics, 11 (3), 03025-1–03025-5. doi: https://doi.org/10.21272/jnep.11(3).03025
48. Subbotina, V., Sobol, O., Belozerov, V., Al-Qawabeha, U. F., Tabaza, T. A., Al-Qawabah, S. M., Shnayder, V. (2020). A study of the electrolyte composition influence on the structure and properties of MAO coatings formed on AMg6 alloy. Eastern-European Journal of Enterprise Technologies, 3 (12 (105)), 6–14. doi: https://doi.org/10.15587/1729-4061.2020.205474
49. Wang, Y., Jiang, Z., Yao, Z. (2009). Microstructure, bonding strength and thermal shock resistance of ceramic coatings on steels prepared by plasma electrolytic oxidation. Applied Surface Science, 256 (3), 650–656. doi: https://doi.org/10.1016/j.apsusc.2009.08.036
50. Wang, Y., Jiang, Z., Yao, Z. (2009). Preparation and properties of ceramic coating on Q235 carbon steel by plasma electrolytic oxidation. Current Applied Physics, 9 (5), 1067–1071. doi: https://doi.org/10.1016/j.cap.2008.12.004